

**Applied Mathematics and Computation**  
**An efficient method for scanned images by using color-correction and L0 gradient minimization**  
--Manuscript Draft--

<b>Manuscript Number:</b>	AMC-D-19-06082
<b>Article Type:</b>	Full Length Article
<b>Section/Category:</b>	65Nxx: partial differential equations, including singularly perturbed differential equation
<b>Keywords:</b>	Color correction ; Image smoothing ; L0 Sparsity ; Fast solver
<b>Corresponding Author:</b>	Yibao Li, Ph.D. Xi'an Jiaotong University Xi'an, CHINA
<b>First Author:</b>	Qing Xia
<b>Order of Authors:</b>	Qing Xia  Zhengyuan Shi  Jing Ji  Yibao Li, Ph.D.
<b>Abstract:</b>	To improve the quality of scanned image captured by cameras, we propose a novel and efficient method for image processing by using color-correction and $L_0$ gradient minimization. Our method is divided into two steps. The first step is to deal with the chromatic aberration. To derive a colorimetric mapping between digital RGB signals and real image values, we use a polynomial modeling by considering the interrelations among the standard color spaces. A $L_0$ gradient minimization is used to remove the image noises. Based on the half-quadratic splitting method, a iterative algorithm for our proposed method is developed and is alternating over a smoothing step. This iterative algorithm is easy to implement and has the optimal complexity $O(N \log N)$ per iteration. Our method is particularly beneficial to correct image color and to remove the noises. Various tests are presented to demonstrate the robustness and efficient of our method.
<b>Suggested Reviewers:</b>	Molada-Tebar Adolfo <a href="mailto:admote@doctor.upv.es">admote@doctor.upv.es</a>  Radoslaw Mantiuk <a href="mailto:rmantiuk@wi.zut.edu.pl">rmantiuk@wi.zut.edu.pl</a>  Chih-Ying Gwo <a href="mailto:ericgwo@uch.edu.tw">ericgwo@uch.edu.tw</a>

**School of Mathematics and Statistics**

Yibao Li

School of Mathematics and Statistics

Xi'an Jiaotong University,

Xi'an 710049,

China

November 23, 2019

***Applied Mathematics and Computation***

Dear Editor:

Please consider the manuscript entitled “**An efficient method for scanned images by using color-correction and  $l_0$  gradient minimization**” authored by Qing Xia, Zhengyuan Shi, Jing Ji and Yibao Li, which we are submitting for consideration for publication in **Applied mathematics and Computation**. We were fully involved in the study and preparation of the manuscript and that the material within has not been and will not be submitted for publication elsewhere.

We look forward to hearing from you with regard to the status of this manuscript and welcome your esteemed comments.

The corresponding author’s information follows: Email is [yibaoli@xjtu.edu.cn](mailto:yibaoli@xjtu.edu.cn) and website is <http://gr.xjtu.edu.cn/web/yibaoli>

Sincerely,

Yibao Li

Associate Professor of School of Mathematics and Statistics

Xi'an Jiaotong University



1 An efficient method for scanned images by using color-correction and  $l_0$  gradient  
2 minimization

3 Qing Xia<sup>a</sup>, Zhengyuan Shi<sup>a</sup>, Jing Ji<sup>b,c</sup>, Yibao Li<sup>a,\*</sup>

4 <sup>a</sup>School of Mathematics and Statistics, Xi'an Jiaotong University, Xi'an 710049, China

5 <sup>b</sup>Xi'an Jiaotong University, State Key Laboratory of Manufacturing Systems Engineering, Xi'an 710049, China

6 <sup>c</sup>Xi'an Jiaotong University Museum, Xi'an Jiaotong University, Xi'an 710049, China

---

7 **Abstract**

To improve the quality of scanned image captured by cameras, we propose a novel and efficient method for image processing by using color-correction and  $l_0$  gradient minimization. Our method is divided into two steps. The first step is to deal with the chromatic aberration. To derive a colorimetric mapping between digital RGB signals and real image values, we use a polynomial modeling by considering the interrelations among the standard color spaces. A  $L_0$  gradient minimization is used to remove the image noises. Based on the half-quadratic splitting method, a iterative algorithm for our proposed method is developed and is alternating over a smoothing step. This iterative algorithm is easy to implement and has the optimal complexity  $O(N \log N)$  per iteration. Our method is particularly beneficial to correct image color and to remove the noises. Various tests are presented to demonstrate the robustness and efficient of our method.

8 **Keywords:** Color correction, Image smoothing,  $L_0$  Sparsity, Fast solver

---

9 **1. Introduction**

10 Images are scanned by the camera into the computer for secondary processing [1, 2, 3]. To obtain a high quality  
11 scanned image, a line scan camera is usually placed in the normal direction to the object surface. When the equipment  
12 starts to work, the reflected light passes through the lens into the line scan camera, which can perform optical-electrical  
13 conversion. After scanning with the camera and comparing with the image acquisition card, the image information is  
14 transferred to the computer for processing and analysis. However, the process of scanning will affect the tone of the  
15 photo and bring noises due to the camera and the external environment. In this paper, our goal is to develop a color  
16 correction method and noises removal method to improve the quality of the scanned image. Figure 1 (a) and (b) show  
17 the exact image and scanned digital image, respectively. With the color corrected method, the image is corrected as  
18 show in Fig. 1(c). With the noised removal method, the quality of the scanned image is improved as shown in Fig.  
19 1(d).

---

\*Corresponding author

Email address: [yibaoli@xjtu.edu.cn](mailto:yibaoli@xjtu.edu.cn) (Yibao Li)

URL: <http://gr.xjtu.edu.cn/web/yibaoli> (Yibao Li)

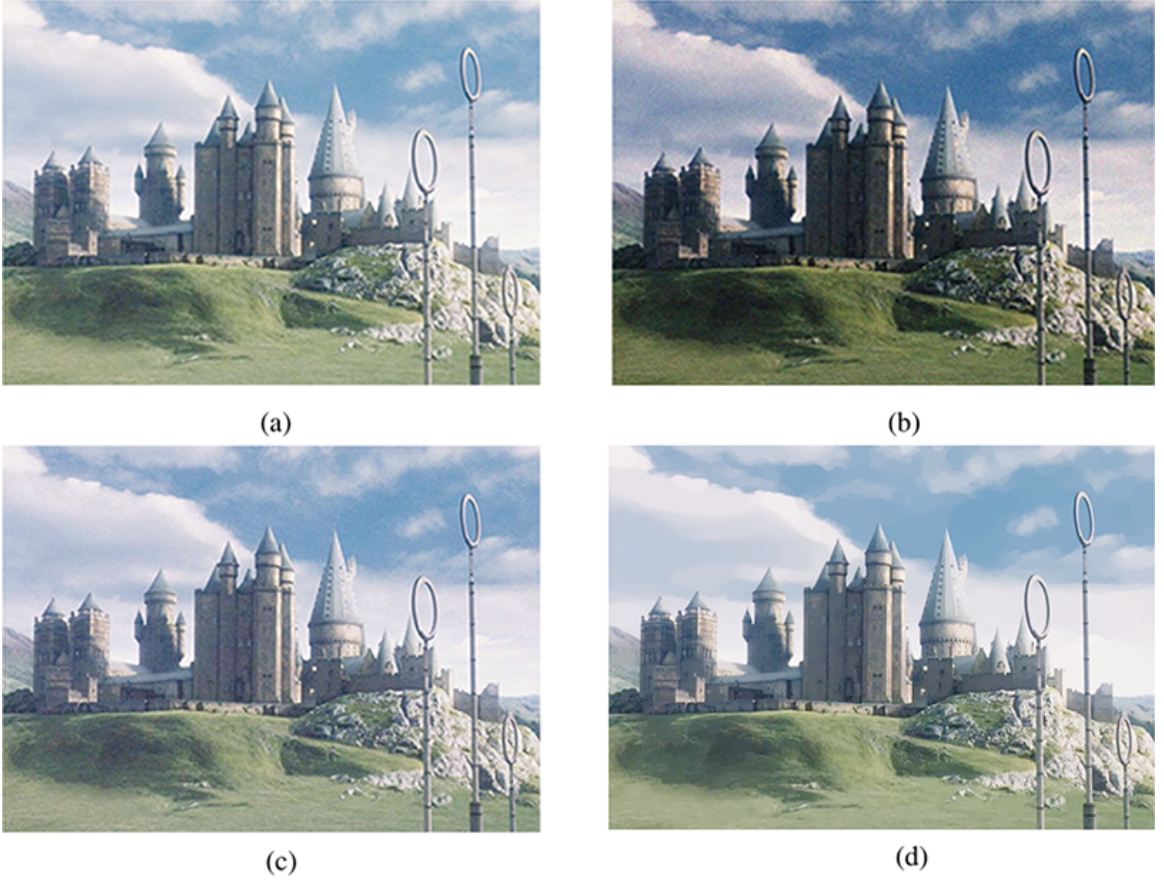


Figure 1: (a) Exact image. (b) Scanned image by using the line scan camera. (c) The color corrected image. (d) The noises removal image .

Generally, the digital camera is firstly used to scan the standard colorimetric card. Then by comparing the pixels values in the standard colorimetric card and the scanned image, a color transforming map can be proposed to transform the scanned image to its exact one. With the proposed map, the color of any scanned image can be corrected[4, 5]. Up to now, many color correction methods have been developed. Hung[6] proposed a look-up-table model to calibrate the pixel color with color chart. Mendes et al.[7] used an efficient colorimetric calibration algorithm for RGB input devices which improves the quality of color recognition in image scanning. Hardeberg et al.[8, 9] introduced a preprocess of polynomial regression in which a cubic root of RGB values is used. Andersen et al.[10] matched digital RGBs to CIEXYZs in each hue slice of color space with different polynomial transformations. Rizzi et al.[11] proposed an heuristic algorithm, which aims to model a simplified version of the inner complex behavior of the human visual system and corrects the images tone. Chen et al.[12] combined the dual-tree complex wavelet in the ridgelet transform and applied it to image denoising. Mantiuk et al.[13] analyzed the color reproduction properties in the tone mapping by extending local and global tone mapping operators.

Meanwhile, various denoising methods were developed. Chan et al.[15] proposed an algorithm for decomposing the image into two regions by minimizing the Mumford-Shah energy function, which works well in processing images

34 with higher noises. Shang.[16] used a determinative basis function as the initialization feature basis function of the  
35 sparse coding algorithm, which improves the efficiency of image denoising. Zibulevsky et al.[14] used  $L_1$  and  $L_2$   
36 norm to solve optimization problem for image denoising. Li et al.[17, 18] used the phase field model for denoising  
37 and keeping the boundary sharp. Shih et al.[19] proposed a parameterized BSVD method that employs the concept  
38 of the SVD for removing the noise, which focus on the relationship between the required peak signal-to-noise ratio  
39 value and the number of singular values to evaluate an optimal threshold of singular values. Gu et al.[20] proposed  
40 a weighted nuclear norm minimization algorithm for image denoising and demonstrated the great potentials in low  
41 level vision applications. Chen et al.[21] used the proximity algorithm to solve the fractional-order TV denoising  
42 model, and provided a particular analysis for the convergence of fractional-order TV denoising method. Abascal  
43 et al.[22] proposed a novel sparse and prior-based algorithm for 3D image denoising, with the additional benefit  
44 of being computationally efficient for application to experimental clinical images. Bubba et al.[23] first proposed  
45 a precise objective function and considered shearlets instead of wavelets. And then they compared the different  
46 regularization terms to choose a better model which provides the desired features of the image. Serafino et al.[24]  
47 considered a smoothed version of TV and proposed a line-search method based on a Huber-like function, which  
48 minimizes a sequence of quadratic models obtained by a second-order Taylor approximation of the KL divergence. For  
49 numerical calculation in image processing, some researchers proposed various acceleration algorithms and methods  
50 in [25, 26, 27, 28].

51 In this paper, we will propose a novel and efficient method to solve the problem of image processing for the  
52 scanned image based on our previous research[29]. In the first step, we set a polynomial regression model to correct the  
53 original tone of a input image. Euclidean distance is used in CIELAB space to evaluate perceptual color differences.  
54 We consider the transformation leading to unsatisfactory results between digital RGB values and the standard CIE  
55 values. Furthermore, the polynomial root terms extension is constructed in our proposed method to further improve  
56 the transformation accuracy. In the second step, we use the  $L_0$  gradient minimization to sharpen prominent edges  
57 and reduce noises. This iterative method is simple and easy to implement. Various numerical tests will be present to  
58 demonstrate the robustness and efficiency of our method.

59 The rest of the paper is organised as follows. In Section 2, we will introduce the transformation between digital  
60 RGB space, stand RGB space, CIEXYZ space and CIELab space. Then we describe the proposed color correct-  
61 ed method and  $L_0$ -smoothing method to remove the noises. Section 3 introduces our numerical solver for the  $l_0$   
62 optimization problem. In Section 4, various experimental results are given. Conclusion is drawn in Section 5.

## 63 2. Methodology

### 64 2.1. Color correction of input images

In this section, we consider the polynomial interrelation among the standard CIE color spaces[30, 31]. First,  
the corresponding tristimulus value is defined as a three dimensional vector  $\mathbf{q}$  ( $\mathbf{q} \in \mathbb{R}^{3 \times 1}$ ) and the device three

dimensional digital response is defined as  $\rho(\rho \in \mathbb{R}^{3 \times 1})$ . A simple linear color characterization transformation can be written as  $\mathbf{M} \cdot \rho = \mathbf{q}$ . Vector  $\rho$  can be extended to  $m$  dimensions by increasing basis function in polynomial regression. We define  $P$  ( $P \in \mathbb{R}^{m \times n}, m \ll n$ ) as a  $m \times n$  matrix of vector  $\rho$  and  $Q$  ( $Q \in \mathbb{R}^{3 \times n}$ ) as the corresponding matrix of vector  $\mathbf{q}$ . The mapping relationship between the camera response space and the corresponding tristimulus value space can be represented by  $M \cdot P = Q$ , where  $M$  is the mapping matrix that depends on  $P$  and  $Q$ . Once the mapping  $M$  is obtained, we can transform any scanned image to its real one. However the standard verify the quality of corrected image [39] is to compute the difference between the real color value  $[L_1 \ a_1 \ b_1]^T$  and the obtained color value  $[L_2 \ a_2 \ b_2]^T$  in CIELAB space as:

$$\Delta E_{ab} = \sqrt{(L_1 - L_2)^2 + (a_1 - a_2)^2 + (b_1 - b_2)^2}. \quad (1)$$

If  $\Delta E_{ab} \in [0 \ 3]$ , the quality of color characterization is very good. If  $\Delta E_{ab} \in (6 \ 10]$ , its quality is sufficient. Otherwise, its quality is insufficient. Our goal is to find the optimal mapping matrix  $M$  keeping the  $\Delta E_{ab}$  be small. The three dimensional vector in  $(\cdot)$  spaces is defined by  $\rho_{(\cdot)}$ . It is well known that there is a linear mapping from CIE 1931 Standard RGB Colorimetric System(RGB) to the CIE 1931 Standard XYZ Colorimetric System(CIEXYZ):

$$\rho_{CIEXYZ} = A \cdot \rho_{RGB}, \quad (2)$$

where

$$A = \begin{bmatrix} 0.49 & 0.31 & 0.2 \\ 0.17697 & 0.81240 & 0.01063 \\ 0.0 & 0.01 & 0.99 \end{bmatrix}. \quad (3)$$

- <sup>65</sup> The transformation relationship between CIEXYZ space ( $\rho_{CIEXYZ} = (X, Y, Z)$ ) and CIE 1931 Standard Lab Col-  
<sup>66</sup> orimetric System(CIELab)( $\rho_{CIELab}$ ) is non-linear:

$$\rho_{CIELab} = N \times \left[ f\left(\frac{X}{X_n}\right), f\left(\frac{Y}{Y_n}\right), f\left(\frac{Z}{Z_n}\right) \right]^T + V \quad (4)$$

where

$$N = \begin{bmatrix} 0 & 116 & 0 \\ 500 & -500 & 0 \\ 0 & 200 & -200 \end{bmatrix}, \quad V = \begin{bmatrix} -16 \\ 0 \\ 0 \end{bmatrix}, \quad \begin{bmatrix} X_n \\ Y_n \\ Z_n \end{bmatrix} = \begin{bmatrix} 96.42 \\ 100 \\ 82.49 \end{bmatrix} \quad (5)$$

and

$$f(a) = \begin{cases} a^{\frac{1}{3}} & \text{if } a \geq 0.008856 \\ 7.787a + \frac{16}{116} & \text{otherwise.} \end{cases} \quad (6)$$

Considering Eqs. (4) and (6), we have

$$\begin{cases} f\left(\frac{X}{X_n}\right) = \left(\frac{X}{X_n}\right)^{\frac{1}{3}} = \left(\frac{2.7689}{X_n}R + \frac{1.7517}{X_n}G + \frac{1.1302}{X_n}B\right)^{\frac{1}{3}} \\ f\left(\frac{Y}{Y_n}\right) = \left(\frac{Y}{Y_n}\right)^{\frac{1}{3}} = \left(\frac{1.0000}{Y_n}R + \frac{4.5907}{Y_n}G + \frac{0.0601}{Y_n}B\right)^{\frac{1}{3}} \\ f\left(\frac{Z}{Z_n}\right) = \left(\frac{Z}{Z_n}\right)^{\frac{1}{3}} = \left(\frac{0.0000}{Z_n}R + \frac{0.0565}{Z_n}G + \frac{5.5943}{Z_n}B\right)^{\frac{1}{3}} \end{cases}. \quad (7)$$

<sup>67</sup> We assume that there exists the new vector  $[(r^*)^{\frac{1}{3}}, (g^*)^{\frac{1}{3}}, (b^*)^{\frac{1}{3}}]^T$  satisfies

$$\begin{bmatrix} \left(\frac{X}{X_n}\right)^{\frac{1}{3}} \\ \left(\frac{Y}{Y_n}\right)^{\frac{1}{3}} \\ \left(\frac{Z}{Z_n}\right)^{\frac{1}{3}} \end{bmatrix} = \begin{bmatrix} \left(\frac{2.7689}{X_n}\right)^{\frac{1}{3}} & \left(\frac{1.7517}{X_n}\right)^{\frac{1}{3}} & \left(\frac{1.1302}{X_n}\right)^{\frac{1}{3}} \\ \left(\frac{1.0000}{Y_n}\right)^{\frac{1}{3}} & \left(\frac{4.5907}{Y_n}\right)^{\frac{1}{3}} & \left(\frac{0.0601}{Y_n}\right)^{\frac{1}{3}} \\ 0.0000 & \left(\frac{0.0565}{Z_n}\right)^{\frac{1}{3}} & \left(\frac{5.5943}{Z_n}\right)^{\frac{1}{3}} \end{bmatrix} \cdot \begin{bmatrix} (r^*)^{\frac{1}{3}} \\ (g^*)^{\frac{1}{3}} \\ (b^*)^{\frac{1}{3}} \end{bmatrix}, \quad (8)$$

<sup>68</sup> where the color characterization transformation is assumed as

$$[(r^*)^{\frac{1}{3}}, (g^*)^{\frac{1}{3}}, (b^*)^{\frac{1}{3}}]^T = \hat{M} \cdot \hat{\rho}(R^{\frac{1}{3}}, G^{\frac{1}{3}}, B^{\frac{1}{3}})^T. \quad (9)$$

<sup>69</sup> Here,  $\hat{\rho}$  is a polynomial regression and  $\hat{M}$  is the mapping matrix. Assume that there exist a  $\check{M}$  which satisfies

$$\hat{\rho}(R^{\frac{1}{3}}, G^{\frac{1}{3}}, B^{\frac{1}{3}}) = \check{M} \cdot \rho(R^{\frac{1}{3}}, G^{\frac{1}{3}}, B^{\frac{1}{3}}). \quad (10)$$

Let  $M = \hat{M} \cdot \check{M}$  and define

$$A^* = \begin{bmatrix} \left(\frac{2.7689}{X_n}\right)^{\frac{1}{3}} & \left(\frac{1.7517}{X_n}\right)^{\frac{1}{3}} & \left(\frac{1.1309}{X_n}\right)^{\frac{1}{3}} \\ \left(\frac{1.0000}{Y_n}\right)^{\frac{1}{3}} & \left(\frac{4.5907}{Y_n}\right)^{\frac{1}{3}} & \left(\frac{0.0601}{Y_n}\right)^{\frac{1}{3}} \\ \left(\frac{0.0000}{Z_n}\right)^{\frac{1}{3}} & \left(\frac{0.0565}{Z_n}\right)^{\frac{1}{3}} & \left(\frac{5.5943}{Z_n}\right)^{\frac{1}{3}} \end{bmatrix}, \quad (11)$$

<sup>70</sup> then we have

$$S = N \cdot A^* \cdot M \cdot P + V. \quad (12)$$

Here  $S$  and  $P$  represent the corresponding matrix of vectors  $\rho_{Lab}$  and  $\rho_{RGB}$ , respectively.  $S$  and  $M$  should be established. However for the standard colorimetric card,  $S$  is known. By solving Eq. (12) based on the training set including digital RGB value and real image value, we have

$$M = (A^*)^{-1} \cdot N^{-1} \cdot (S - V) \cdot P^T / (P \cdot P^T). \quad (13)$$

<sup>71</sup> Once we obtain the mapping  $M$ , we can transform any scanned image to its real one as following steps:

<sup>72</sup> • Step 1: Using Eq. (12), we compute  $S$ .

<sup>73</sup> • Step 2: Using Eq. (4), we calculate  $\rho_{CIEXYZ}$ .

<sup>74</sup> • Step 3: Using Eq. (2), we obtain the real image  $\rho_{RGB}$ .

<sup>75</sup> After these three steps, the quality of the scanned image can be improved.

76    2.2. *L<sub>0</sub>-smoothing with noise image*

For a 2D image representation, we define  $I(\mathbf{x})$  as the color corrected image and  $\phi(\mathbf{x})$  as the smoothing result based on  $I$ . We consider the following  $l_0$  gradient regularization version:

$$\min_{\phi} \int_{\Omega} \|(I(\mathbf{x}) - \phi(\mathbf{x}))\|_2^2 + \beta \|\nabla \phi(\mathbf{x})\|_0 d\mathbf{x} \quad (14)$$

77 where  $\|\cdot\|_2$  is the  $L_2$  norm. The term  $\|(I(\mathbf{x}) - \phi(\mathbf{x}))\|_2^2$  enforces  $\phi$  be similar with color corrected  $I$ . Let us briefly  
 78 review the definition of  $L_0$ -norm: if  $\phi = 0$ , then  $\|\phi\|_0 = 0$ . Otherwise,  $\|\phi\|_0 = 1$ . therefore the term  $\|\nabla \phi(\mathbf{x})\|_0$  can  
 79 reduce the noises and make edges sharpen. It is worth pointing out that  $L_0$ -norm regularized optimization problem is  
 80 known as computationally intractable. Recently, an algorithm for directly optimizing the  $L_0$ -norm was proposed in  
 81 the context of image processing [32] and surface denoising [33]. This optimization problem (Eq. (14)) is equivalent  
 82 minimize the following equation:

$$G = \|(I(\mathbf{x}) - \phi(\mathbf{x}))\|_2^2 + \beta \|\nabla \phi(\mathbf{x}) - \psi(\mathbf{x})\|_2^2 + \lambda \|\psi(\mathbf{x})\|_0. \quad (15)$$

83 Here we introduce a new parameter  $\psi$  in the optimization problem.  $\beta$  is a weight directly controlling the similarity  
 84 between  $\psi$  and the gradient of  $\phi$ . We can divide the optimization problem of  $G$  into two equations as:

$$G_1 = \min_{\psi} \lambda \|\psi\|_0 + \beta \|\nabla \phi(\mathbf{x}) - \psi\|_2^2 \quad \text{with fixed } \phi \quad (16)$$

$$G_2 = \min_{\phi} \|(I(\mathbf{x}) - \phi(\mathbf{x}))\|_2^2 + \beta \|\nabla \phi(\mathbf{x}) - \psi\|_2^2 \quad \text{with fixed } \psi \quad (17)$$

For Eq. (16), we should consider the definition of  $\|\cdot\|_0$  on the optimization problem with fixed  $\phi$ . We define  $G_1^*$  as the minimum of Eq. (16). Considering Eq. (16), if  $\lambda = 0$ , we can obtain the minimum of  $G_1$  by setting  $\psi = \nabla \phi$ , otherwise we need to analyze the relationship between  $\|\nabla \phi(\mathbf{x})\|_2^2$  and  $\lambda/\beta$ . The relations are summarized as follows:

1) When  $\|\nabla \phi(\mathbf{x})\|_2^2 \geq \lambda/\beta$ , we start splitting in the following two situations. In the first situation, by considering  $\psi \neq 0$ , we can obtain the minimal value  $G_1^*$  by setting  $\nabla \phi(\mathbf{x}) = \psi$  shown as

$$G_1^*(\psi \neq 0) = \min_{\psi} G_1(\psi \neq 0) = \lambda \|\psi\|_0 + \beta \|\nabla \phi - \psi\|_2^2 = \lambda \quad (18)$$

For the second situation  $\psi = 0$ , we can obtain

$$G_1^*(\psi = 0) = \min_{\psi} G_1(\psi = 0) = \lambda \|\psi\|_0 + \beta \|\nabla \phi - \psi\|_2^2 = \beta \|\nabla \phi\|_2^2 \geq \lambda = \min_{\psi} G_1(\psi \neq 0) \quad (19)$$

Therefore, we should only let  $\nabla \phi = \psi$  to obtain the minimum  $G_1^*$ . In conclusion, combining Eqs. (18) and (19), the minimum energy (16) is produced when  $\nabla \phi = \psi$ .

2) When  $\|\nabla \phi(\mathbf{x})\|_2^2 < \lambda/\beta$ , in a similar way we obtain

$$G_1^*(\psi \neq 0) = \min_{\psi} G_1(\psi \neq 0) = \lambda \quad (20)$$

and

$$G_1^*(\psi = 0) = \min_{\psi} G_1(\psi = 0) = \beta \|\nabla \phi\|_2^2 \quad (21)$$

Combining Eqs. (20) and (21), we can find  $G_1^*(\psi = 0)$  is smaller than  $G_1^*(\psi \neq 0)$ . The minimum  $G_1^* = \beta \|\nabla \phi\|_2^2$  reaches by choosing  $\psi$  is 0. In summary, to minimize Eq. (16), we can obtain the following condition:

$$\psi = \begin{cases} \nabla \phi & \text{if } \lambda = 0 \text{ or } \|\nabla \phi\|_2^2 \geq \frac{\lambda}{\beta} \\ 0 & \text{otherwise} \end{cases} \quad (22)$$

85 Equation (17) is a quadratic function which has a global minimum even by gradient descent with fixed  $\psi$ :

$$-\phi + \beta \Delta \phi = -I + \beta \nabla \cdot \psi \cdot x \quad (23)$$

86 **3. Numerical solver**

87 We employ the fast scheme with the Fourier-spectral method [34]. We assume that there are  $N_x \times N_y$  pixels on  
88 a 2D image, where  $N_x$  and  $N_y$  are even integers. Let  $x_m = (2m - 1)/2$ ,  $y_n = (2n - 1)/2$ , for  $1 \leq m \leq N_x$ ,  
89  $1 \leq n \leq N_y$ . Furthermore, let  $\phi_{mn}^s$  be an approximation of  $\phi(x_m, y_n, s)$ , where  $s$  is the iterative step. The discrete  
90 cosine transform  $\hat{\phi}_{pq}^s$  for  $p = 1, \dots, N_x$ ,  $q = 1, \dots, N_y$  is defined as

$$\hat{\phi}_{pq}^s = \alpha_p \beta_q \sum_{m=1}^{N_x} \sum_{n=1}^{N_y} \phi_{mn}^s \cos(x_m \pi \xi_p) \cos(y_n \pi \eta_q),$$

91 where

$$\alpha_p = \begin{cases} \sqrt{1/N_x}, & p = 1 \\ \sqrt{2/N_x}, & 2 \leq p \leq N_x \end{cases} \quad \text{and} \quad \beta_q = \begin{cases} \sqrt{1/N_y}, & q = 1 \\ \sqrt{2/N_y}, & 2 \leq q \leq N_y \end{cases}$$

92 The variables  $\xi_p$  and  $\eta_q$  are defined as  $\xi_p = (p - 1)/N_x$  and  $\eta_q = (q - 1)/N_y$ , respectively. The inverse discrete  
93 cosine transform is

$$\phi_{mn}^s = \sum_{p=1}^{N_x} \sum_{q=1}^{N_y} \alpha_p \beta_q \hat{\phi}_{pq}^s \cos(\xi_p \pi x_m) \cos(\eta_q \pi y_n). \quad (24)$$

It is easy to solve  $\psi^{s+1}$  from  $\phi^s$  and  $\beta^s$  by using Eq. (22) as

$$\psi^{s+1} = \begin{cases} \nabla \phi^s & \|\nabla \phi^s\|_2^2 \geq \frac{\lambda}{\beta^s} \\ 0 & \text{otherwise} \end{cases} \quad (25)$$

94 Once  $\psi^{s+1}$  is obtained, we find that the Eq. (23) for the  $\phi$  at the step  $(s + 1)$ :

$$-\phi_{mn}^{s+1} + \beta^s \Delta \phi_{mn}^{s+1} = -I_{mn} + \beta^s \nabla \cdot \psi_{mn}^{s+1}. \quad (26)$$

95 Thus, Eq. (26) can be transformed into the discrete cosine space as follows:

$$-(1 + \beta^s [(\xi_p \pi)^2 + (\eta_q \pi)^2]) \hat{\phi}_{pq}^{s+1} = -\hat{I}_{pq} + i \beta^s (\xi_p \pi + \eta_q \pi) \hat{\phi}_{pq}^s$$

96 Here  $i = \sqrt{-1}$  is a complex number and we have employed the discrete cosine transform for the Laplacian and  
 97 divergence operators, which are defined as

$$\Delta \hat{\phi}_{pq} = -((\xi_p \pi)^2 + (\eta_q \pi)^2) \hat{\phi}_{pq} \text{ and } \nabla \cdot \hat{\psi}_{pq} = i(\xi_p \pi + \eta_q \pi) \hat{\psi}_{pq}.$$

98 Furthermore,  $\hat{I}_{pq}$  and  $\hat{\psi}_{pq}$  denote the discrete cosine transform of  $I_{mn}$ , and  $\psi_{mn}$ . Therefore, we obtain the following  
 99 discrete cosine transform

$$\hat{\phi}_{pq}^{s+1} = \frac{\hat{I}_{pq} - i\beta^s(\xi_p \pi + \eta_q \pi)\hat{\phi}_{pq}^s}{1 + \beta^s(\xi_p \pi)^2 + \beta^s(\eta_q \pi)^2}. \quad (27)$$

100 The corresponding function  $\phi_{mn}^{s+1}$  can be computed using Eq. (24). The outline of the main procedure in one time step  
 101 is as follows.

102 *Step 1.* Initialize  $\phi^0$  and  $\lambda, \beta = \beta^0$ .

103 *Step 2.* Solve  $\psi^{s+1}$  from  $\phi^s$  and  $\beta^s$  by using Eq. (25).

104 *Step 3.* Solve  $\phi^{s+1}$  from  $\psi^{s+1}$  by using Eqs. (27) and (24):

105 *Step 4.* Update  $\beta^{s+1} = \kappa\beta^s$ , where  $\kappa$  is larger than 1 to make  $\beta$  increase with each iteration.

106 The main contributions of the proposed method include the following. (i) The proposed method can improve the  
 107 quality of scanned images without artificial noises because it uses the color-correction and  $l_0$  gradient minimization;  
 108 (ii) the proposed numerical method in Eqs. (25) and (27) can achieve fast convergence, since our algorithm consists  
 109 of two explicit evaluations of the closed-form solutions and one implicit Poisson type equation solver. (iii) For the  
 110 linear equation, their computational complexities are  $O(N)$ , where  $N$  is the size of the mesh grid. For the implicit  
 111 Poisson type equation solver, we apply a fast discrete cosine transform method with a computational complexity of  
 112  $O(N \log N)$ . Our proposed numerical scheme can be straightforwardly applied to GPU-accelerated DCT implemen-  
 113 tation that performs up to many times faster than CPU-only alternatives; and (iv) the proposed algorithm is simple to  
 114 implement.

#### 115 4. Experimental results

116 In this section, we present numerical results on various synthetic and real images. Figure 2 shows the cultural relics  
 117 images. Due to the long preservation time of cultural relics, the difficulty of scanning increases and the brightness and  
 118 saturation of scanned images decreases as shown in Fig. 2(b). Comparing with Fig. 2(a), our proposed method has  
 119 performed well in relics color correction as shown in Fig. 2(c). Here, we choose  $\beta = 0.02$  and  $\kappa = 2$ .

120 To verify the performance of our method, we tested our method with the public data and carried out camera  
 121 experiments under both ideal and actual light sources. For each set of data, we compared the results of our proposed  
 122 method with other methods mentioned. The parameters for evaluating the method performance include the mean  
 123  $\Delta E_{ab}$  color difference for all color samples  $\Delta E_{ab}$ , the maximum  $\Delta E_{ab}$  color difference  $\Delta E_{max}$ , the mean error of  
 124 each color attribute  $\Delta L, \Delta a, \Delta b$ , the maximum error of each color attribute  $\Delta L_{max}, \Delta a_{max}, \Delta b_{max}$ . We consider  
 125 two data sets. One data set is obtained from the AGFA Arcus II scanner with the AGFA IT8.7/2 color chart. This data

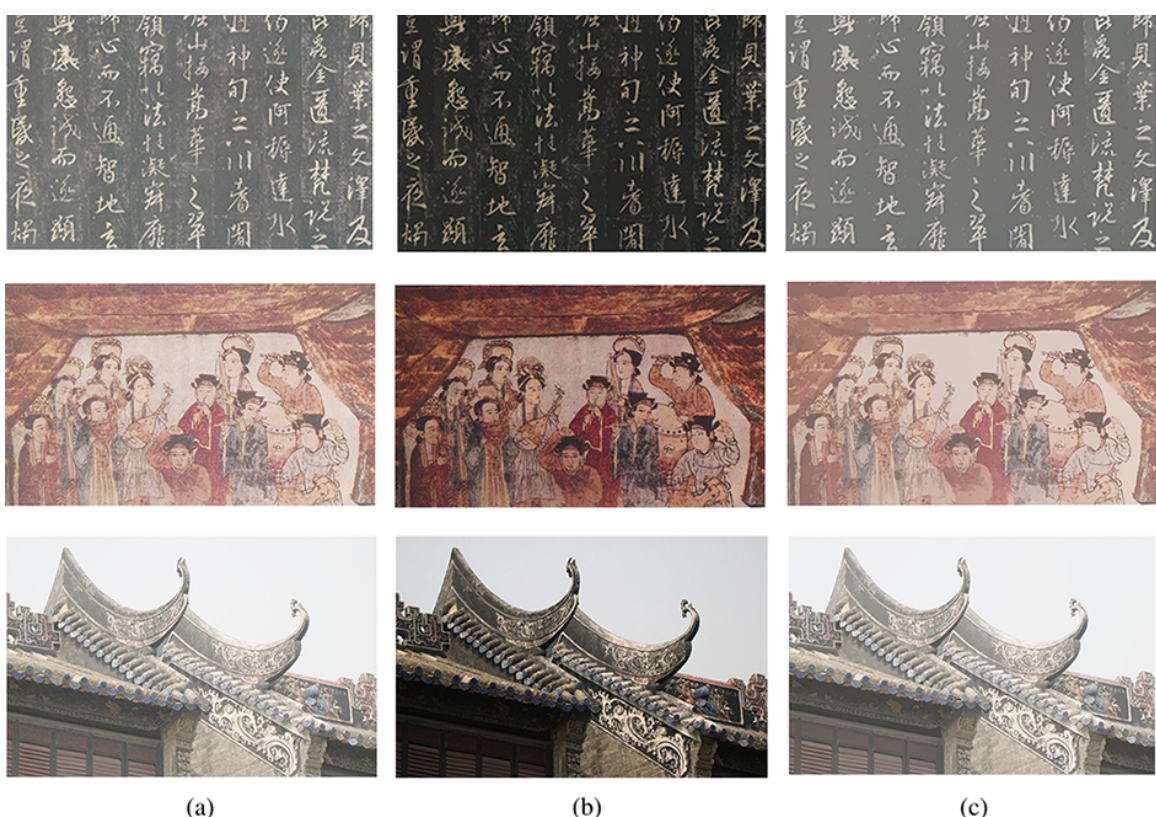


Figure 2: Color correction of our proposed method. (a) Original image. (b) Digital image captured by camera. (c) Our results.

126 set is given in the appendix of the literature [8] proposed by Hardeberg. The other data set is obtained under the ideal  
 127 light source. Here Nikon D200 camera is applied to capture the image of the X-Rite IT8.7/2 color checker which is  
 128 positioned in the ColorSpace cabinet and lit by the D65 metamer illuminant.

129 Table 1 and Table 2 show the results obtained by using the methods with RGB–CIEXYZ [35], RGB–CIELAB [37],  
 130 Hardeberg [8], and our method on the two mentioned data sets. Observing these results, we can see that the direct  
 131 transformation from digital RGB values to CIELAB space does not provide better results than that from digital RGB  
 132 values to CIEXYZ space, instead, the results get worse. This is because the conversion from CIEXYZ to CIELAB is  
 133 non-linear, involving a cubic root function. But in our method, the color conversion is derived reversely considering  
 134 the nature of color space transformations, so clearly better results are obtained.

Table 1: Data given in the literature experiment results

Model type	$\overline{\Delta E}$	$\Delta E_{max}$	$\overline{\Delta L}$	$\Delta L_{max}$	$\overline{\Delta a}$	$\Delta a_{max}$	$\overline{\Delta b}$	$\Delta b_{max}$
RGB–CIEXYZ[35]	4.841	22.939	1.276	3.715	2.782	20.932	3.135	15.354
RGB–CIELAB[37]	22.270	49.111	15.310	34.052	8.422	37.251	9.056	40.062
Hardeberg[8]	5.652	23.961	3.241	11.345	2.234	23.304	2.987	12.645
<b>Our method</b>	<b>1.0130</b>	<b>4.7816</b>	<b>0.3417</b>	<b>2.5473</b>	<b>0.5691</b>	<b>3.3129</b>	<b>0.5913</b>	<b>3.3891</b>

Table 2: Ideal light source experiment results

Model type	$\overline{\Delta E}$	$\Delta E_{max}$	$\overline{\Delta L}$	$\Delta L_{max}$	$\overline{\Delta a}$	$\Delta a_{max}$	$\overline{\Delta b}$	$\Delta b_{max}$
RGB–CIEXYZ[35]	4.4162	12.4252	1.7173	7.0779	2.5783	9.0875	2.4828	10.3337
RGB–CIELAB[37]	6.5634	14.4275	3.6462	9.5623	4.0434	9.1865	4.5145	12.6367
Hardeberg[8]	4.1482	10.5636	1.2825	6.7647	2.4636	8.5632	2.2413	9.3883
RPCC[36]	4.5687	12.9247	1.8975	7.5459	2.6586	9.1158	2.5048	10.7479
<b>Our method</b>	<b>2.2016</b>	<b>8.9461</b>	<b>1.1057</b>	<b>4.4196</b>	<b>0.9728</b>	<b>5.5157</b>	<b>1.2968</b>	<b>6.9315</b>

135 In the top of Fig. 3(a)-(d), we add the gaussian noises with 1%, 5%, 15% and 25% into a synthetic image acquisi-  
 136 tion card, respectively. The added noise satisfies the Gaussian distribution with expectation of 0 and variance of 0.01.  
 137 The given probability r% means setting a fraction of r% randomly selected pixels to noises. The bottom row shows  
 138 the denoising results with our method. Here, we choose the interface parameter  $\beta = 0.005, 0.01, 0.015$ , and  $0.015$   
 139 , $\kappa = 4.5, 4, 2.4$ , and 2, respectively. We can see that our proposed method successfully remove the noises of the  
 140 images. Furthermore, as shown in Fig. 3(a-c), our method can keep the sharpen edge when the noise is small. While  
 141 the too higher noise leads the edges be over-smooth.

142 Figure 4 shows the results comparison with different norms in energy function with bronze ware image. Fig. 4(a)

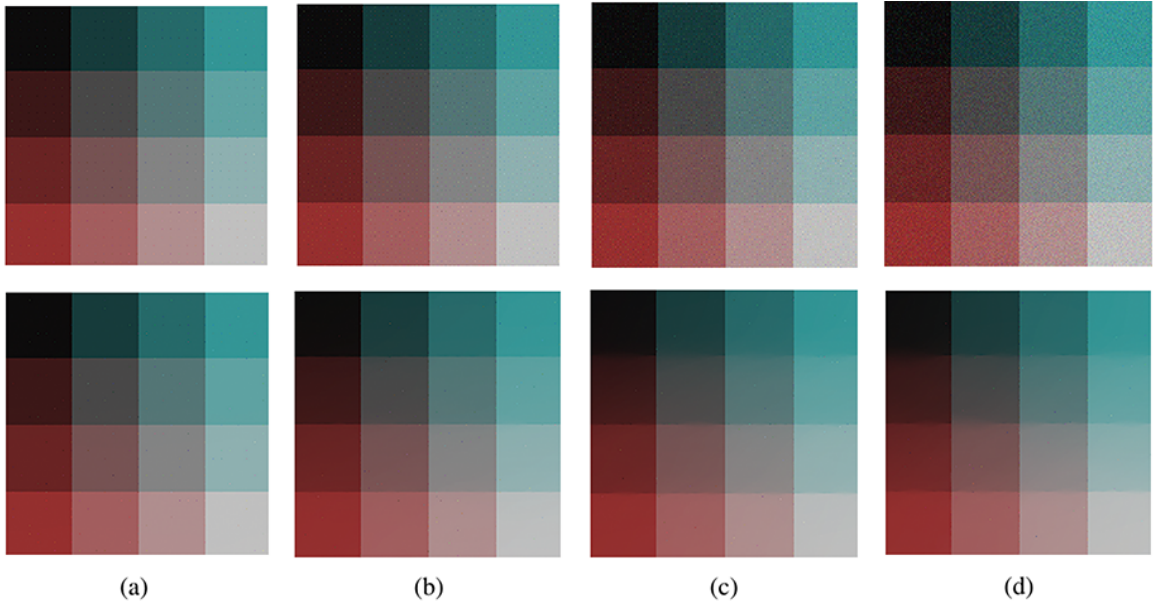


Figure 3: The top row shows original image with gaussian noise which expectation is 0 and variance is 0.01. The bottom row shows the denoising results with our method. From (a) to (d), the proportions of noise in the images are 1%, 5%, 15% and 25%, respectively.

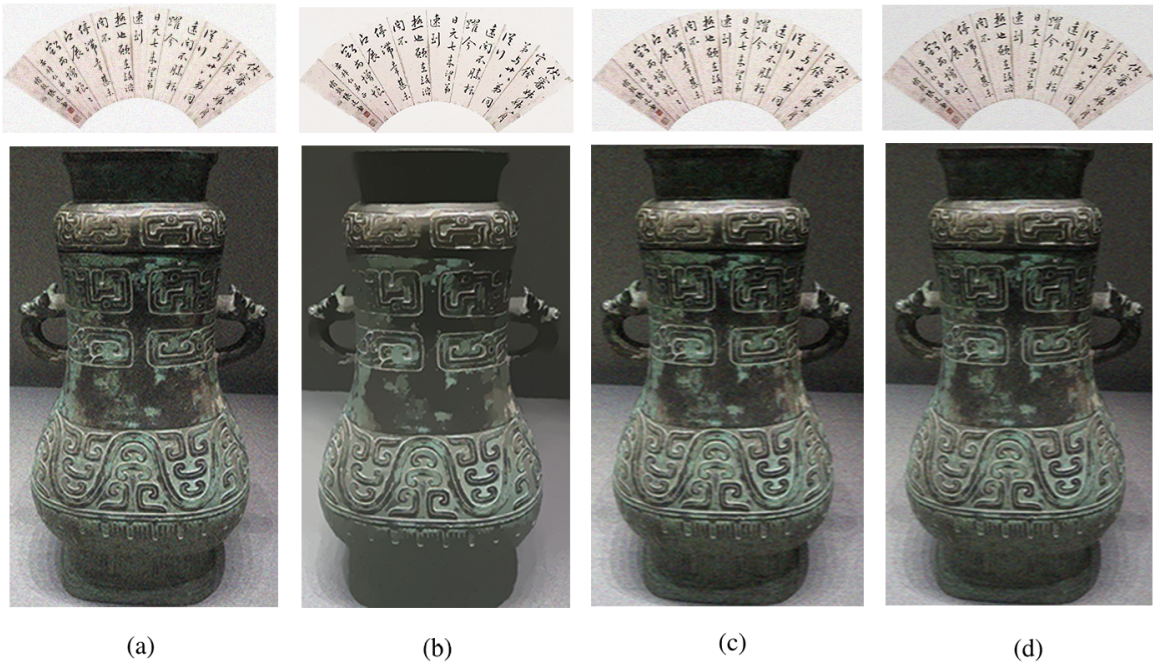


Figure 4: Results with different norms in energy function with bronze ware image. (a) Initial image with gaussian noise. (b)-(d) Results of minimization energy function with  $L_0$ ,  $L_1$  and  $L_2$  norm.

143 is the original image with gaussian noise. From Fig. 4(b-d), we use  $L_0$ ,  $L_1$  and  $L_2$  norms in the energy function  
 144 minimization (Eq. (14)), respectively. In our algorithm, we choose  $\beta = 0.01$  and  $\kappa = 1.85$ . Note that we have used  
 145 an iterated soft-thresholding algorithm for  $L_1$  as introduced in [38]. It is worth pointing out that  $L_1$  and  $L_2$  norms  
 146 homogenizes the noise in the image which makes the original image blurred. However,  $L_0$  norm can enhance the  
 147 contrast of image and suppress low-amplitude details.

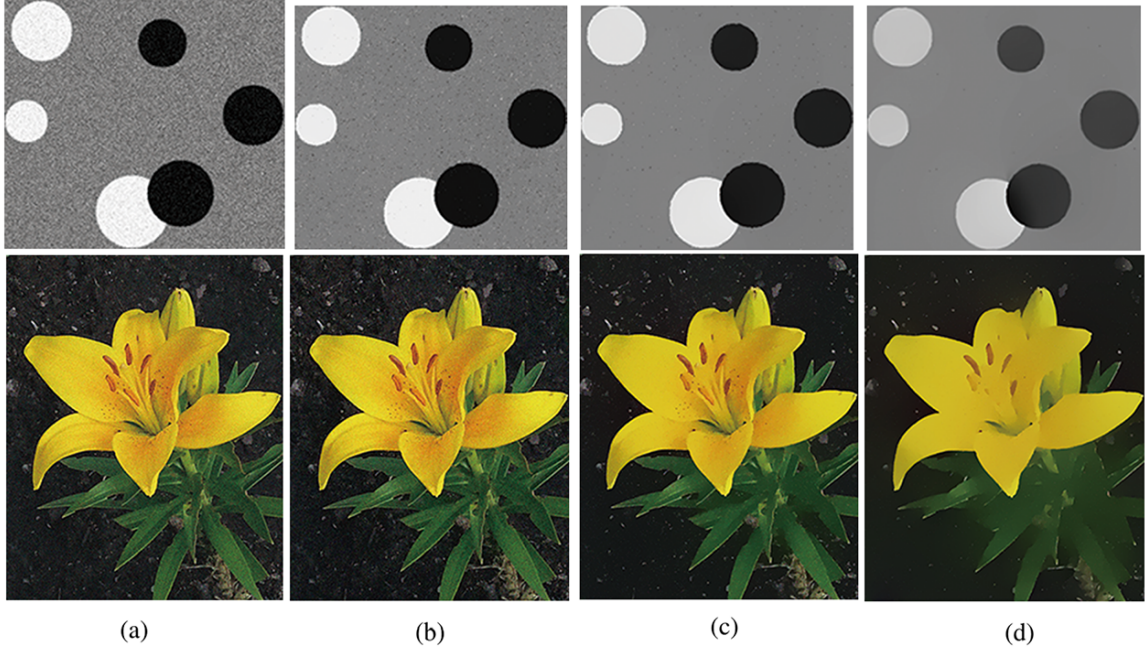


Figure 5: Result comparison with quantization and denoising. (a) The image with noise. (b-d) The denoising parameters are  $\beta = 0.02$ ,  $0.04$  and  $0.08$ , respectively. Here  $\kappa = 2$  is fixed.

148 In Fig. 5, we present a synthetic image and a real image with noises in first and second rows, respectively. In  
 149 order to ignore the influence of iteration step, we set  $\kappa = 2$  for every image. The denoising results parameters  
 150  $\beta = 0.02$ ,  $0.04$ , and  $0.08$  are used in Fig. 5(b-d), respectively. As can be observed, the noises of the images will be  
 151 reduced and the texture will be improved gradually. For the synthetic image, because there is no influence of texture,  
 152 Fig. 5(d) with  $\beta = 0.08$  has a good result. For the real image, Fig. 5(c) has a better result because it is closer to the  
 153 authentic scene.

154 Figure 6 shows the comparison results by different iterations with fix  $\beta = 0.02$ , which shows our proposed  
 155 method performed well by increasing iterations with fix  $\beta$ . In this figure, we use various types of images, which are  
 156 hand-writing image, gray-scale image, color image and real culture relic image, respectively, to verify the robustness  
 157 of proposed method. From (b) to (e), we choose  $\kappa$  as  $4.50$ ,  $1.65$ ,  $1.35$  and  $1.24$ , which represent  $10$  iterations,  $30$   
 158 iterations,  $50$  iterations and  $70$  iterations, respectively. As can be seen in Fig. 6(d) and (e), our method has eliminated  
 159 most of noise and sharpen the edge. Meanwhile, choosing adaptive  $\beta$  can lead to better results.

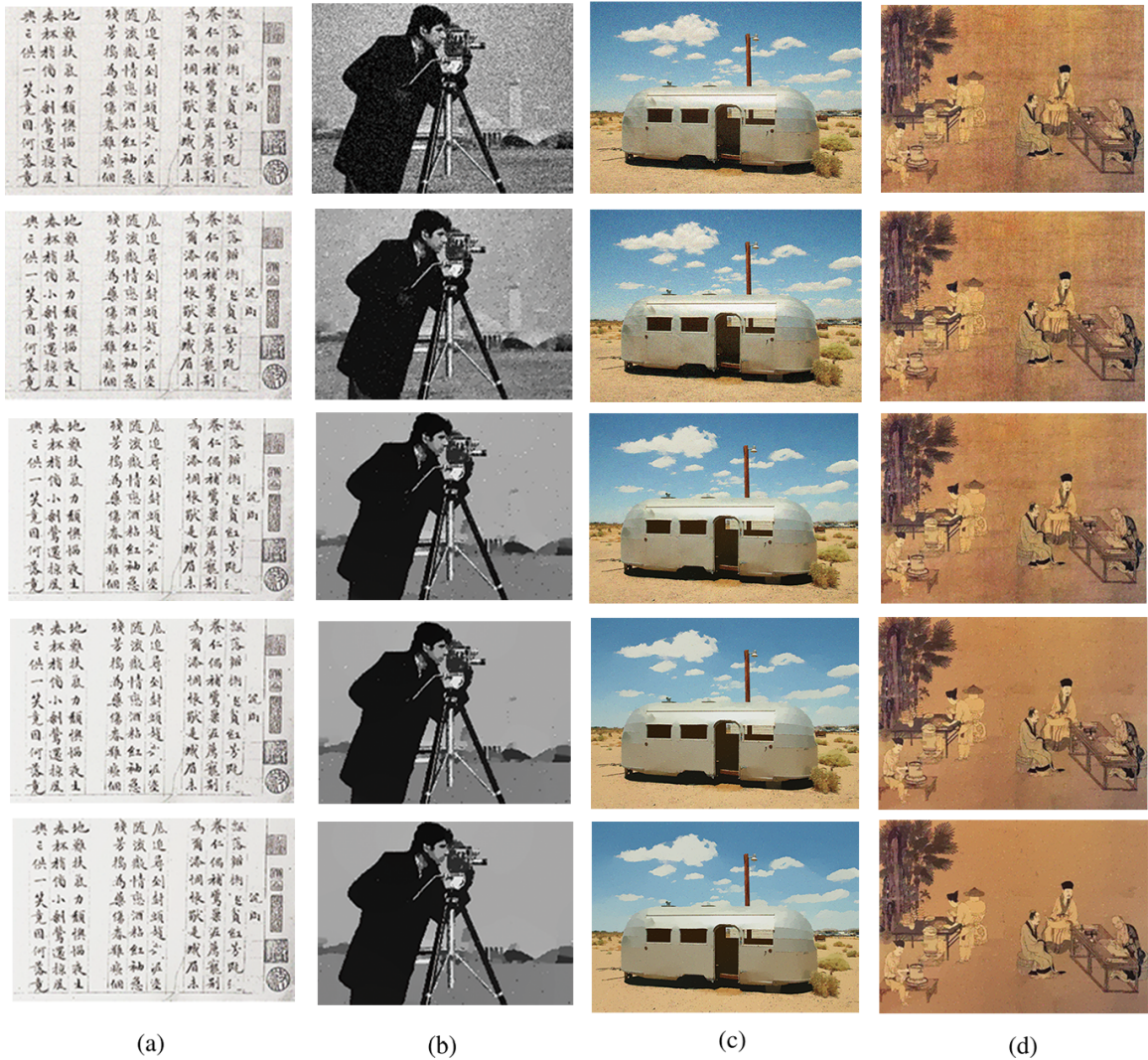


Figure 6: Comparison results by different iterations with  $\beta = 0.02$ . (a) is the original images with gaussian noise. From left to right, we use hand-writing image, gray-scale image, color image and real culture relic image to test the effect of our method, respectively. From (b) to (e), the results are the images with 10 iterations( $\kappa = 4.5$ ), 30 iterations( $\kappa = 1.65$ ), 50 iterations( $\kappa = 1.35$ ) and 70 iterations( $\kappa = 1.25$ ), respectively.

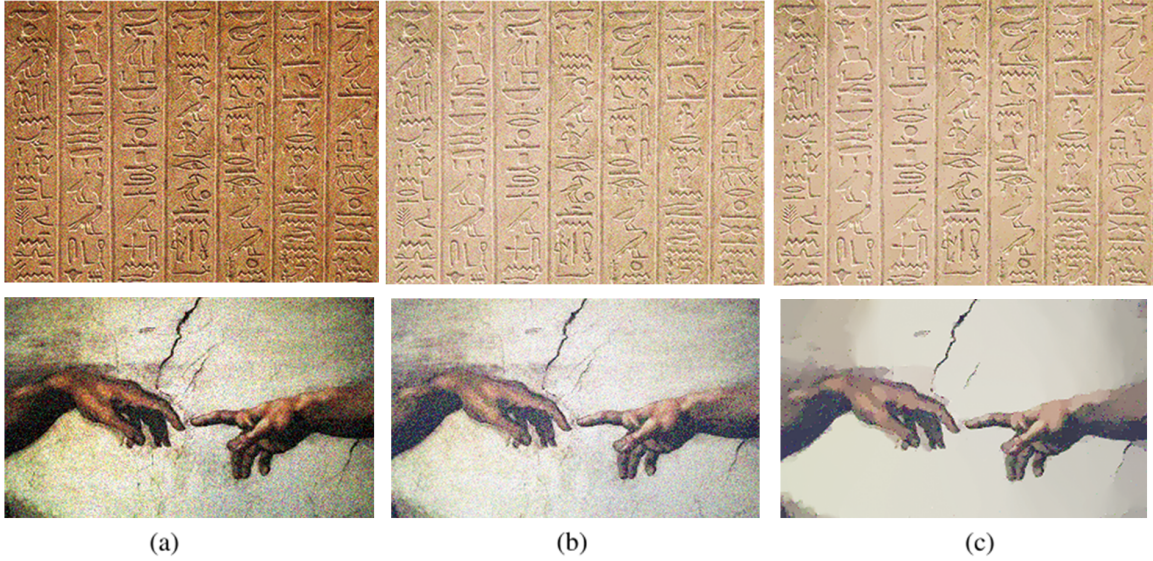


Figure 7: Full processing of real scanned images with hieroglyphical characters in ancient Egypt and ancient Roman fresco. (a) are the scanned images with affected tone and noise. (b) are the results of color corrected images with noise. (c) are the final results with corrected color and noise.

160 In the final test, we use the several real scanned images as shown in Fig. 7. From Fig. 7(a), we correct the color  
 161 of the images and get the clear results in Fig. 7(b), which have even color character and the contrast is obvious. Here  
 162 we choose the smooth parameter  $\beta = 0.01$ , and run the simulation up to 20 iterations to get the denoising ancient  
 163 Egypt in Fig. 7(c). For denoising ancient Roman fresco in Fig. 7, we choose  $\beta = 0.01$  and  $\kappa = 1.65$ . In Fig. 7(c),  
 164 the contents of the cultural relics have been highlighted and the noises are reduced, except for the damaged parts. As  
 165 can be seen, our algorithm disposes the relics images well.

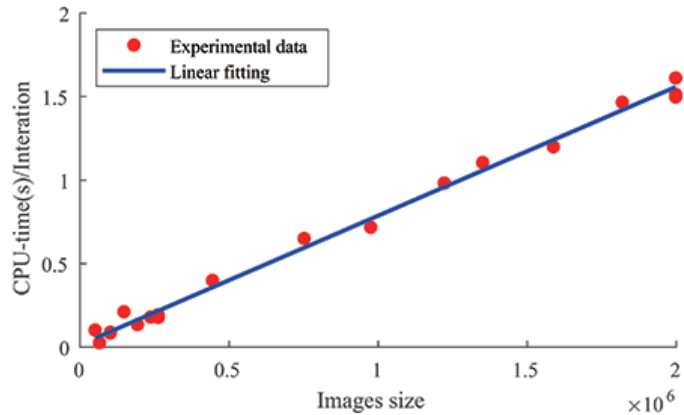


Figure 8: Experimental data and linear fitting average CPU time per iteration versus image size.

166 Finally, we show the performance of all test problems. We calculate the average CPU time per iteration (total CPU  
 167 time over total iterations) and fit the curve with images size as shown in Fig. 8. Here, the linear fitting is done using  
 168 the MATLAB function polyfit. It can be seen that the convergence rate of the computational cost is linear with respect

169 to images size. Therefore our method is simple and fast.

170 **5. Conclusion**

171 In this paper, we have presented a novel robust and efficient method for image processing using color-correction  
172 and  $L_0$  gradient minimization, which gives an obvious improvement in color characterization accuracy and removes  
173 noise of the images. Our method can be improved in several ways. First, we can extend the polynomial root terms  
174 to further improve the transformation of color correction accuracy. The results presented in this paper show that  
175 this algorithm outperforms linear regression and offers a significant improvement over polynomial models when the  
176 exposure/scene irradiance varies. The polynomial root terms extension is constructed in our proposed method to  
177 further improve the transformation accuracy. Then, automatically adapting parameters of  $L_0$  minimization can get  
178 sharper features and eliminate noises. Unlike other denoising methods with  $L_1$  or  $L_2$  norm, our method can remove  
179 low-amplitude pixels and globally preserve and enhance salient edges, even if they are boundaries of very narrow  
180 objects. This iterative algorithm is easy to implement and computational efficient. Various tests are presented to  
181 demonstrate that our method is robust and produces good image processing results.

182 **Conflict of interests**

183 The authors declare that there is no conflict of interests regarding the publication of this article.

184 **Acknowledgment**

185 Y.B. Li is supported by National Natural Science Foundation of China(No.11601416), the Fundamental Research  
186 Funds for the Central Universities (No.XTR042019005) and the China Postdoctoral Science Foundation (No.2018M640968).

187 **Reference**

- 188 [1] A. Molada-Tebar, J.L. Lerma, A. Marques-Mateu, Camera characterization for improving color archaeological documentation, *Color Res. Appl.* 43 (14) (2017) 47–57.  
189 [2] M. Barni, A. Pelagotti, A. Piva, Image processing for the analysis and conservation of paintings: opportunities and challenges, *IEEE Signal Proc Mag.* 22 (5) (2005) 141–144.  
190 [3] R. Parry, Digital heritage and the rise of theory in museum computing, *Mus. Manag. Curator.* 20 (4) (2005) 333–348.  
191 [4] G. Sharma, H.J. Trussell, Digital color imaging, *IEEE T. Image. Process.* 7 (6) (1993) 901–932.  
192 [5] G.D. Finlayson, S.D. Hordley, Color constancy at a pixel, *J. Opt. Soc. Am A.* 2 (18) (2001) 253–264.  
193 [6] P.C. Hung, Colorimetric calibration in electronic imaging devices using a look-up table model and interpolations, *Electronic Imag.* 2 (1) (1993) 53–61.  
194 [7] L. Mendes, P. Carvalho, Adaptive polynomial regression for colorimetric scanner calibration using genetic algorithms, *Proceedings of the IEEE International Workshop on Intelligent Signal Processing* (2005), pp. 22–27.  
195 [8] J.Y. Hardeberg, Acquisition and reproduction of colour images: colorimetric and multispectral approaches, Doctoral Thesis. 1999.

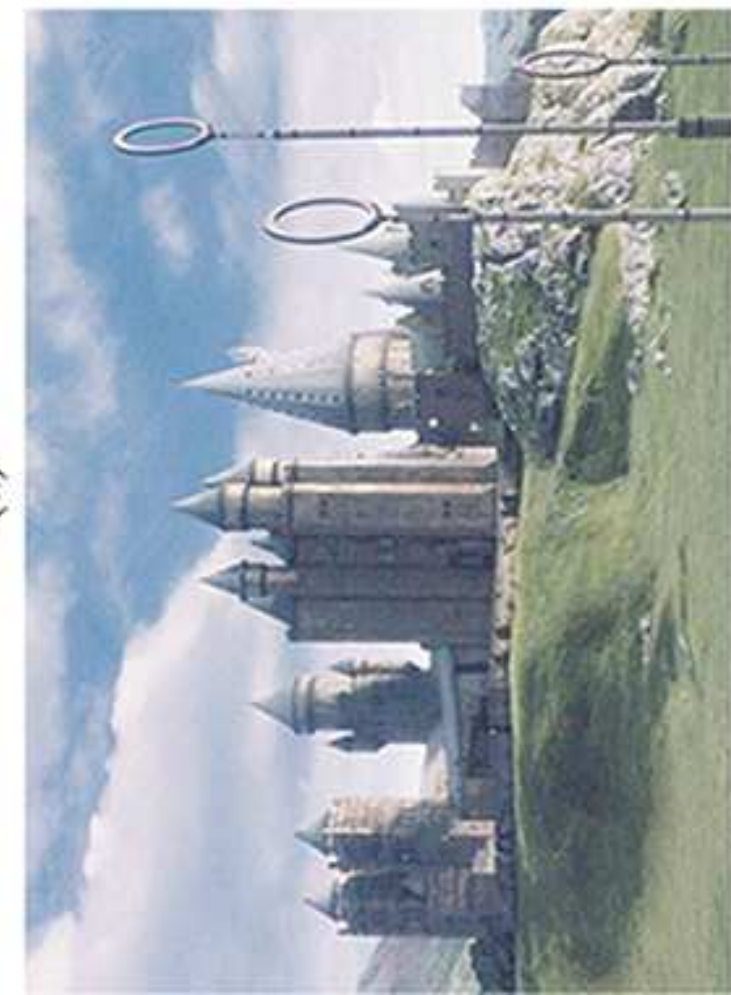
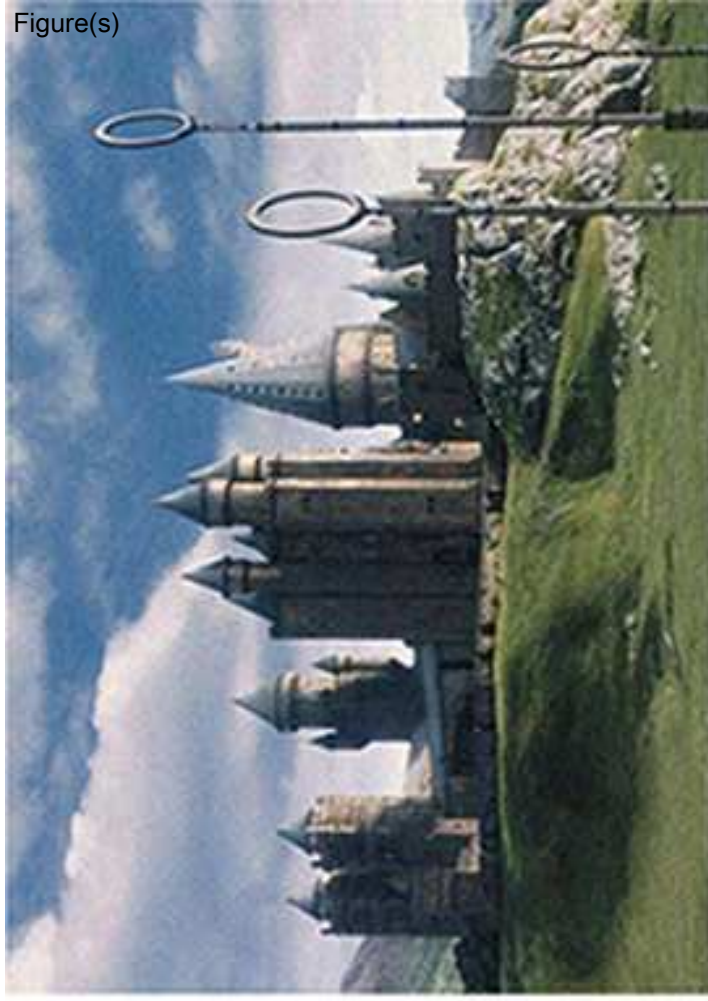
- 200 [9] J.Y. Hardeberg, F. Schmitt, I. Tastl, H. Brettel, J.P. Crettez, Color management for color facsimile. In Proc. IST and SIDs 4th Color Imaging  
201 Conf.: Color Science, Systems and Applications, Scottsdale. (1996) 108–113.
- 202 [10] C.F. Andersen, J.Y. Hardeberg, Colorimetric characterization of digital cameras preserving hue planes, In: Proc. 13th Color Imag. Conf.  
203 (2005) 141–146.
- 204 [11] A. Rizzi, C. Gatta, D. Marini, A new algorithm for unsupervised global and local color correction, Pattern Recogn. Lett. 24 (2003) 1663C–  
205 1677.
- 206 [12] G.Y. Chen, B. Kgl, Image denoising with complex ridgelets, Pattern Recogn. 40 (2007) 578–585.
- 207 [13] R. Mantiuk, R. Mantiuk, A. Tomaszewska, W. Heidrich, Color correction for tone mapping, Comput Graph Forum. 28 (2009) 193–202.
- 208 [14] M. Zibulevsky, M. Elad,  $L_1$ - $L_2$  optimization in signal and image processing, IEEE Signal Proc Mag. 27 (3) (2010) 76–88.
- 209 [15] T. Chan, L. Vese, Active contours without edges, IEEE Trans. Image Process. 10 (2) (2001) 266–277.
- 210 [16] L. Shang, Denoising natural images based on a modified sparse coding algorithm, Appl. Math. Comput. 205 (2008) 883–889.
- 211 [17] Y. Li, J. Kim, Multiphase image segmentation using a phase-field model, Comput. Math. Appl. 62 (2011) 737–745.
- 212 [18] Y. Li, J. Kim, An unconditionally stable hybrid method for image segmentation, Appl. Numer. Math. 82 (2014) 32–43.
- 213 [19] Y.T. Shih, C.S. Chien, C.Y. Chuang, An adaptive parameterized block-based singular value decomposition for image de-noising and com-  
214 pression, Appl. Math. Comput. 218 (2012) 10370–10385.
- 215 [20] S. Gu, L. Zhang, W. Zuo, X. Feng, Weighted nuclear norm minimization with application to image denoising, Proc. IEEE Conf. Comput. Vis.  
216 Pattern Recognit., pp. 2862–2869, Jun. 2014.
- 217 [21] D. Chen, Y.Q. Chen, D. Xue, Fractional-order total variation image denoising based on proximity algorithm, Appl Math Comput. 257 (2015)  
218 537–545.
- 219 [22] J.F.P.J. Abascal, S. Si-Mohamed, P. Douek, C. Chappard, F. Peyrin, A sparse and prior based method for 3D image denoising, HAL-02056591.  
220 2019.
- 221 [23] T.A. Bubba, F. Porta, G. Zanghirati, S. Bonettini, A nonsmooth regularization approach based on shearlets for Poisson noise removal in ROI  
222 tomography, Appl. Math. Comput. 318 (2018) 131–152.
- 223 [24] D.D. Serafino, G. Landi, M. Viola, ACQUIRE: an inexact iteratively reweighted norm approach for TV-based Poisson image restoration,  
224 Appl. Math. Comput. 364 (2020) 124678.
- 225 [25] F. Daz, H. Montero, D. Santana, G. Montero, E. Rodríguez, L. Mazorra Aguiar, A. Oliver, Improving shadows detection for solar radiation  
226 numerical models, Appl. Math. Comput. 319 (2018) 71–85.
- 227 [26] A.W. Deng, C.Y. Gwo, Fast and stable algorithms for high-order Pseudo Zernike moments and image reconstruction, Appl. Math. Comput.  
228 334 (2018) 239–253.
- 229 [27] X. Sun, P. Dang, Numerical stability of circular Hilbert transform and its application to signal decomposition, Appl. Math. Comput. 359  
230 (2019) 357–373.
- 231 [28] M.A.D.S. Lourenco, E.L.M. Padilla, An octree structured finite volume based solver, Appl. Math. Comput. 365 (2020) 124721.
- 232 [29] J. Ji, S. Fang, Zhengyuan Shi, Qing Xia, Yibao Li, An efficient non-linear polynomial color characterization method based on interrelations  
233 of color spaces, In review.
- 234 [30] L.L. Weatherall, B.D. Coombs, Skin color measurements in terms of CIELAB color space values, J. Inverst. Dermatol. 4 (99) (1992) 468–473.
- 235 [31] C. Connolly, T. Fleiss, A study of efficiency and accuracy in the transformation from RGB to CIELAB color space, IEEE T. Image Process.  
236 7 (6) (1997) 1046–1048.
- 237 [32] L. Xu, C. Lu, Y. Xu, J. Jia, Image smoothing via  $L_0$  gradient minimization, ACM Trans. Graph. 30 (6) 174.
- 238 [33] Y. Sun, S. Schaefer, W. Wang, Denoising point sets via  $L_0$  minimization, Comput. Aided. Geom. D. 35–36 (2015) 2–15.
- 239 [34] G. Sheng, T. Wang, Q. Du, K.G. Wang, Z.K. Liu, L.Q. Chen, Coarsening kinetics of a two phase mixture with highly disparate diffusion  
240 mobility, Commun. Comput. Phys. 8 (2010) 249–264.
- 241 [35] G. Hong, M.R. Luo, P.A. Rhodes, A study of digital camera colorimetric characterization based on polynomial modeling, Color Res. Appl.  
242 26 (1) (2001) 76–84.

- 243 [36] G.D. Finlayson, M. Mackiewicz, A. Hurlbert, Color correction using root-polynomial regression, IEEE T. Image. Process. 24 (5) (2015)  
244 1460–1470.
- 245 [37] B. Sun, H. Liu, S. Zhou, W. Li, Evaluating the performance of polynomial regression method with different parameters during color charac-  
246 terization, Math. Probl. Eng. 2014 (1) (2014) 1–7.
- 247 [38] M. Schmidt, G. Fung, R. Rosales, Fast optimization methods for  $L_1$  regularization: a comparative study and two new approaches, Proc. 18th  
248 European Conf. on Machine Learning (ECML), September 2007, Warsaw, Poland, pp. 286–297.
- 249 [39] A. Abrardo, V. Cappellini, M. Cappellini, A. Mecocci, Art-works colour calibration using the VASARI scanner, Proc. 4th IS&T/SID Color  
250 Imaging Conf., 94 (1996).



Click here to access/download  
**LaTeX Source Files**  
image\_processing\_L0\_CIE3.0.tex





見葉之文澤及  
以象金匱流梵說之  
印遂使阿難達水  
迎神句之川者閑  
於山為萬華之年  
鎮寫法性深解集  
而不通智地玄  
身康懶滅而遙顯  
是謂重鑒之祐

見葉之文澤及  
以象金匱流梵說之  
印遂使阿難達水  
迎神句之川者閑  
於山為萬華之年  
鎮寫法性深解集  
而不通智地玄  
身康懶滅而遙顯  
是謂重鑒之祐

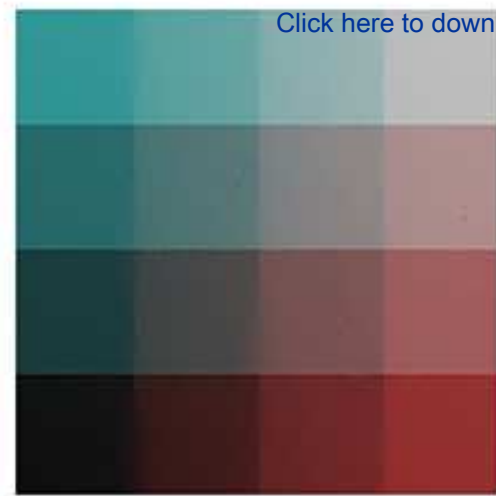
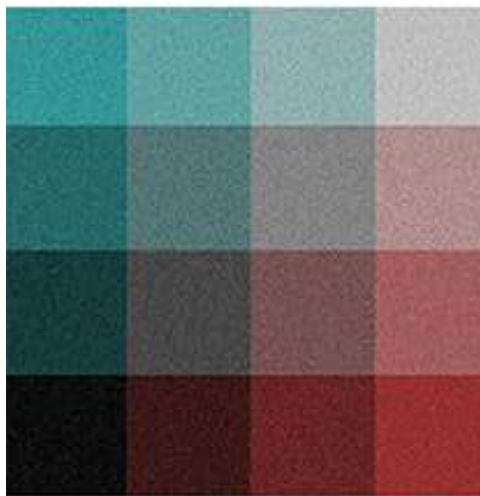
見葉之文澤及  
以象金匱流梵說之  
印遂使阿難達水  
迎神句之川者閑  
於山為萬華之年  
鎮寫法性深解集  
而不通智地玄  
身康懶滅而遙顯  
是謂重鑒之祐



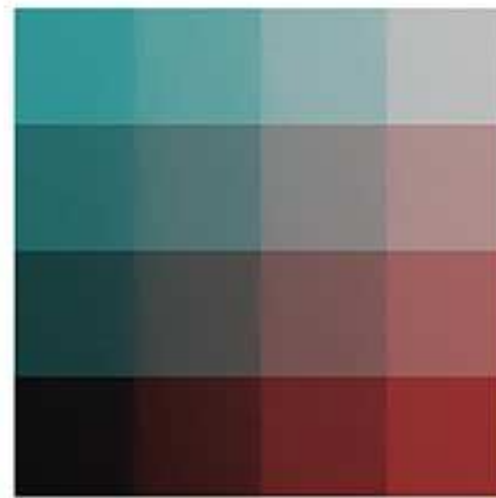
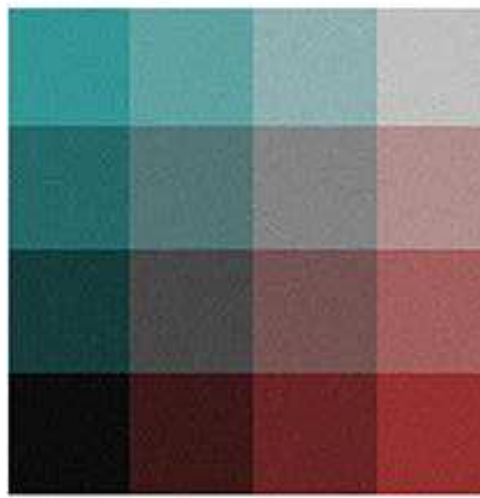
(c)

(b)

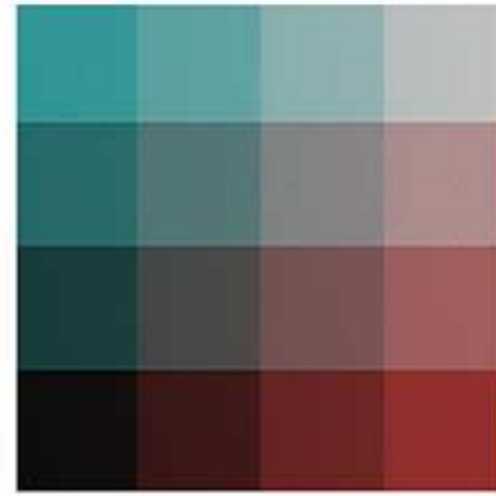
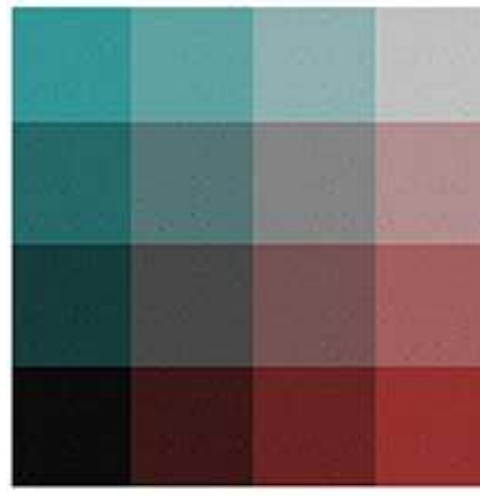
(a)



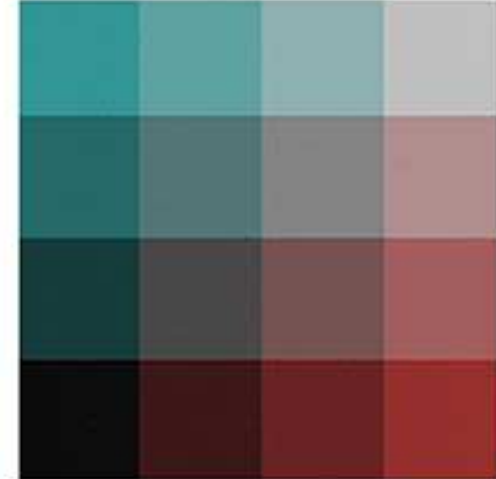
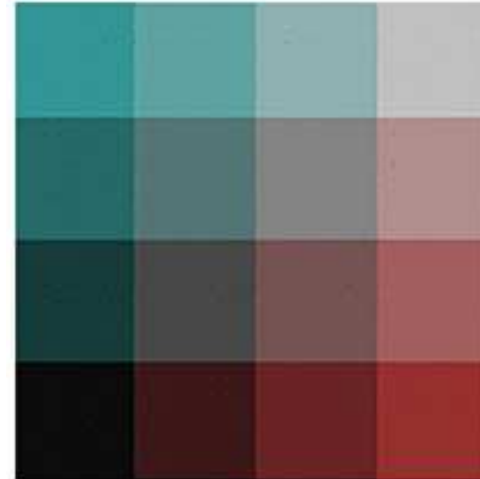
(d)



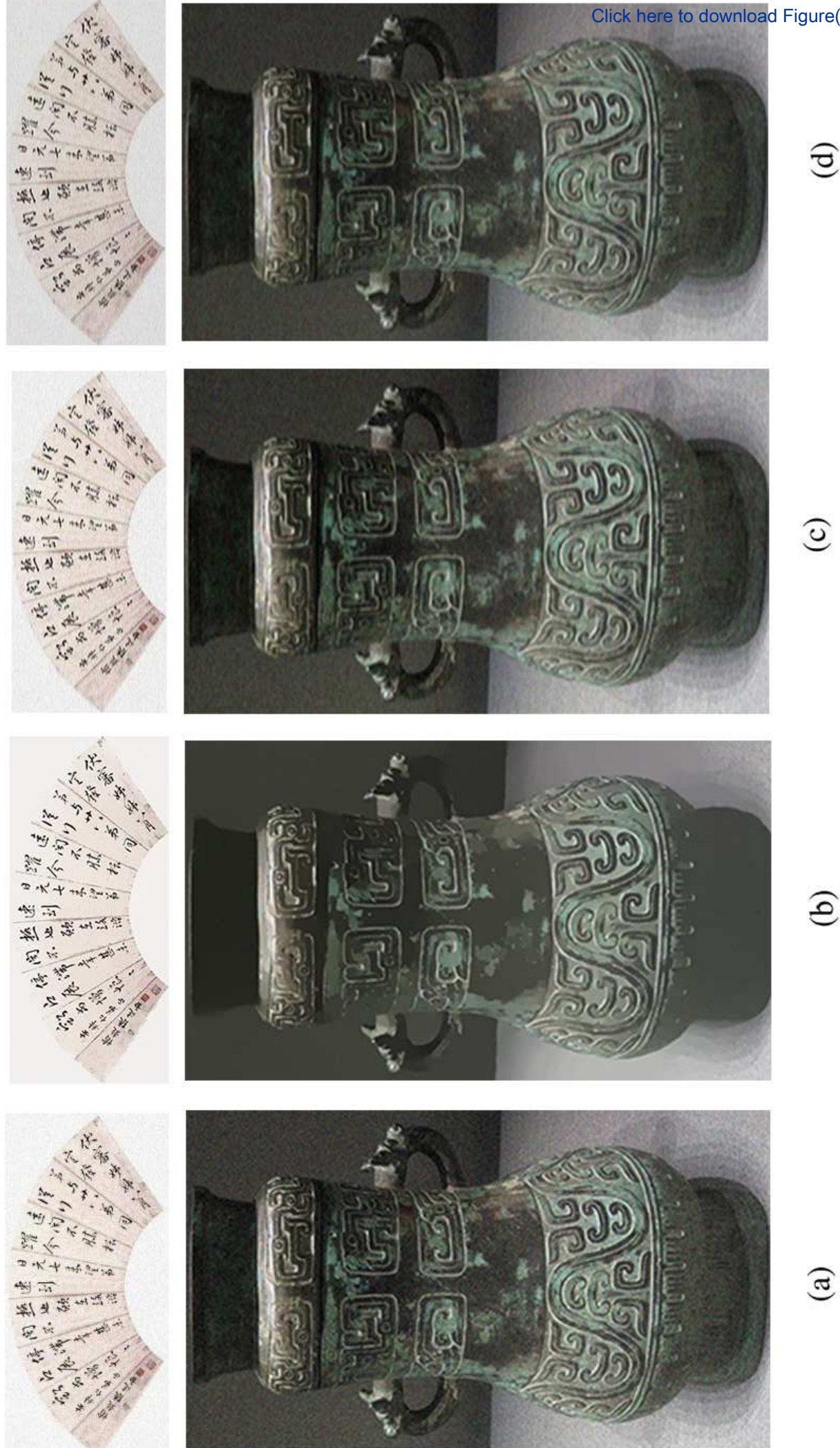
(c)

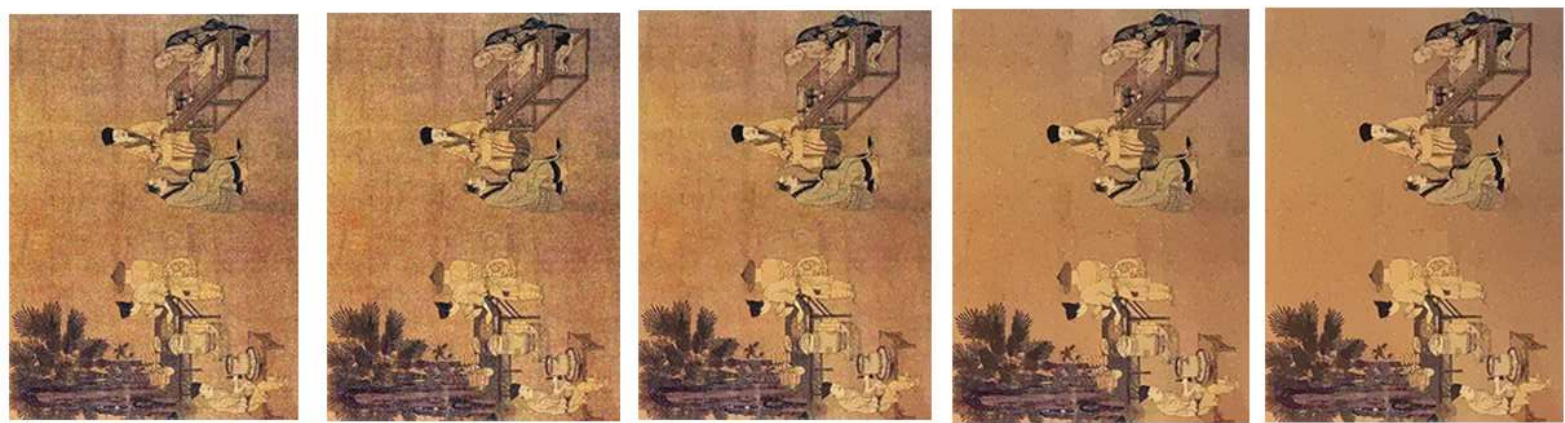


(b)

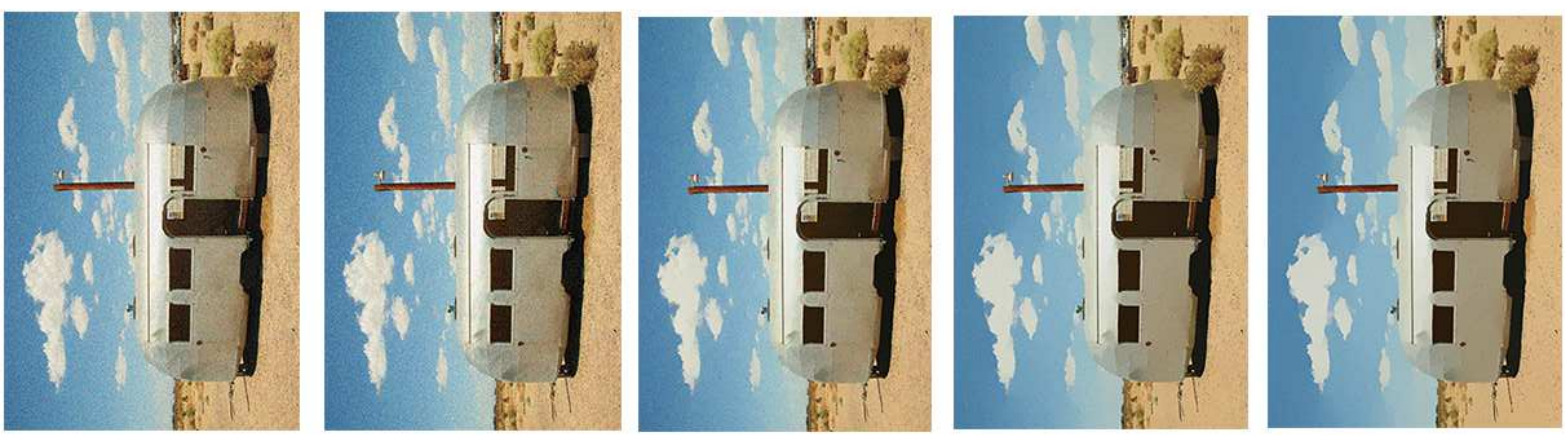


(a)

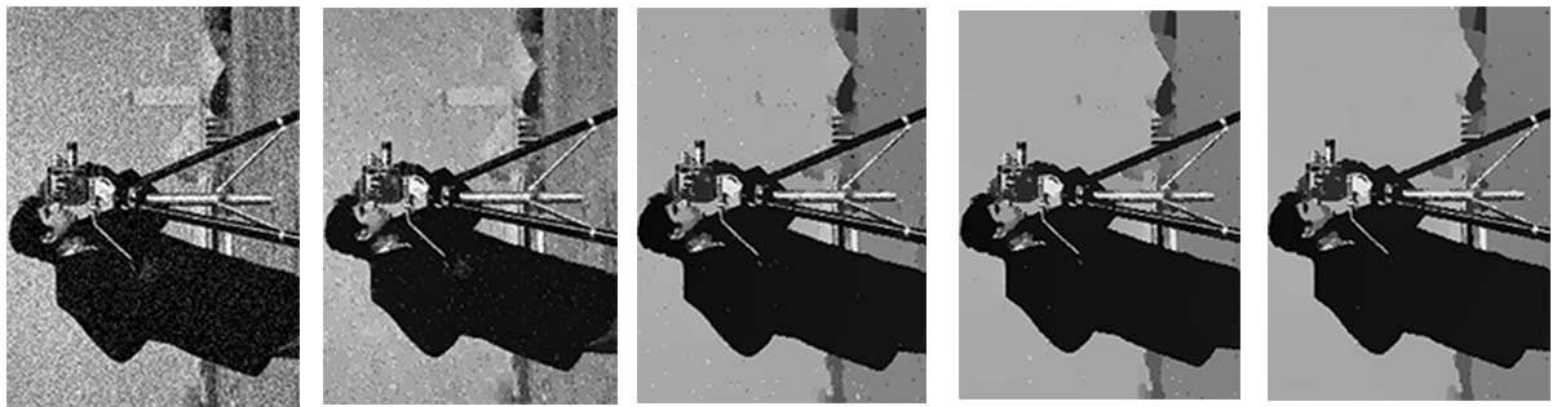




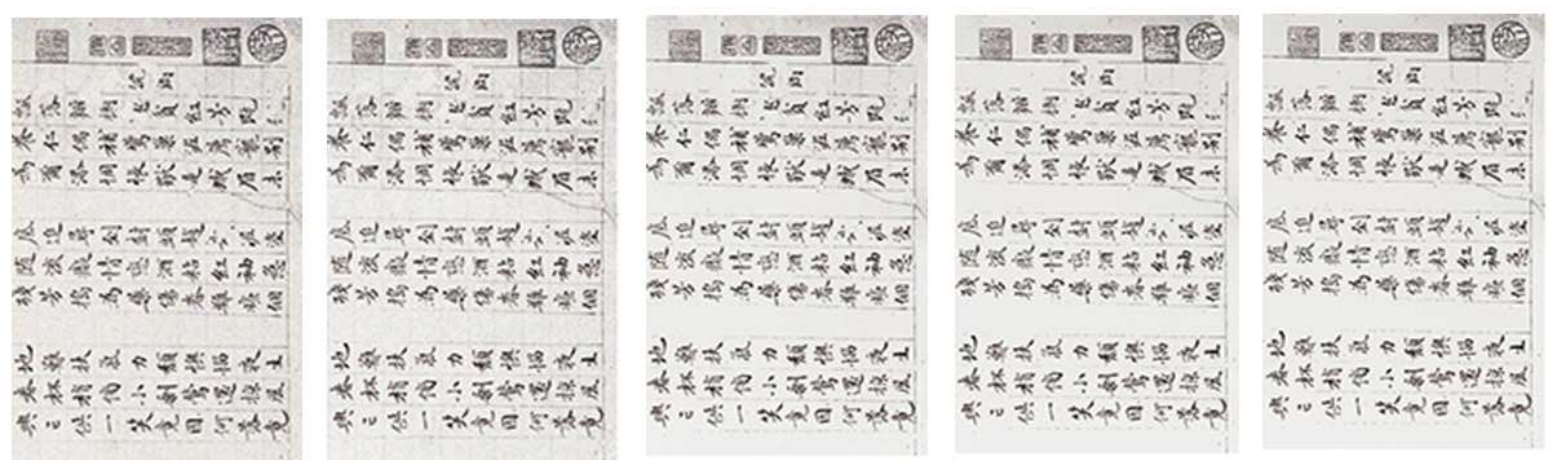
(d)



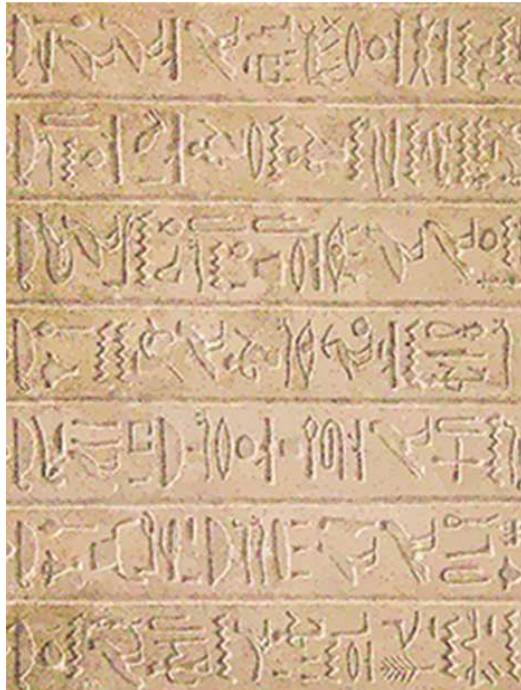
(c)



(b)



(a)



(c)



(b)



(a)

